Coupling of the VAMPER permafrost model within the earth system model *i*LOVECLIM (version 1.0): description and validation

D. Kitover, R. van Balen, D.M. Roche, J. Vandenberghe, H. Renssen

Earth and Climate Cluster, Faculty of Earth and Life Sciences, Vrije Universiteit Amsterdam, Amsterdam, the Netherlands

Correspondence to: D.C. Kitover (d.c.kitover@vu.nl)

Abstract

The VAMPER permafrost model has been enhanced for coupling within the *i*LOVECLIM earth system model of intermediate complexity by including snow thickness and active layer calculations. In addition, the coupling between *i*LOVECLIM and the VAMPER model includes two spatially variable maps of geothermal heat flux and generalized lithology. A semi-coupled version is validated using the modern day extent of permafrost along with observed permafrost thickness and subsurface temperatures at selected borehole sites. The modeling run not including the effects of snow cover overestimate the present permafrost extent. However, when the snow component is included, the extent is overall reduced too much. It was found that most of the modeled thickness values and subsurface temperatures fall within a reasonable range of the corresponding observed values. Discrepancies are due to lack of captured effects from features such as topography and organic soil layers. In addition, some discrepancy is also due to disequilibrium with the current climate, meaning that some permafrost is a result of colder states and therefore cannot be reproduced accurately with the *i*LOVECLIM preindustrial forcings.

1 Introduction

The **VU Am**sterdam **Per**mafrost (VAMPER) model is a deep 1-d heat conduction model with phase change capability. At a number of arctic/subarctic locations, the model has simulated both equilibrium and transient permafrost depth estimates (Kitover et al., 2012; Kitover et al., 2013). The model was built with the intention to couple it within *i*LOVECLIM, an earth system model of intermediate complexity. Although the VAMPER model simulations have been previously validated and forced using climate model data, a common technique for modeling permafrost, the next step is to build on these developments, providing the ability to investigate the permafrost-climate relationship. Therefore, VAMPER has been enhanced so that it may be more realistically coupled within *i*LOVECLIM. With this coupling, it is the ultimate goal to capture the transient nature of permafrost growth/decay over millennia as a feedback effect during major periods of climate change. However, as a first step, the VAMPER model has been semi-coupled to ECBilt, the atmospheric module that includes the land component within *i*LOVECLIM, to validate the simulation of modern-day permafrost extent and thickness. We use the term semi-coupled since the coupling is only one-directional (from ECBilt to VAMPER). In other words, the effects of (changing) permafrost are not fed back to the climate. The goal

of this paper is to describe this coupling and then analyze the validation experiment for modeling present-day permafrost, with detailed explanation of why mismatches occur between simulated and observed data.

The first example of VAMPER as a stand-alone deep permafrost model was for Barrow, Alaska (Kitover et al., 2012) where the experiment simply reproduced the present-day permafrost depth using monthly averaged observation data of ground "surface" (- 1 cm deep) temperatures. In this same study, VAMPER was also validated by comparing results against other developed deep permafrost models (also used for millennial-scale simulations) using similar forcings and parameter settings. In both Kitover et al. (2012) and Kitover et al. (2013), a number of transient simulations at selected locations (e.g. Wyoming, West Siberia, Central Siberia) were performed using the stand-alone version of the VAMPER model, forced by *i*LOVECLIM-generated air surface temperatures over the last 21k years (Roche et al., 2011). In addition, a sensitivity analysis was presented in Kitover et al. (2013), showing the range of simulated permafrost depths under different parameter settings.

Thus far, according to the work summarized above, VAMPER has only been employed as a post-processing , site-specific permafrost model. However, the advantage of the model being simple with limited parameterization requirements, hence resulting in speedy computation times, have not been fully realized since it is not yet coupled within *i*LOVECLIM. As a next step, this paper describes the necessary developments to couple VAMPER with ECBilt, the atmospheric component of *i*LOVECLIM, via the air surface temperature. Specifically, this presented work introduces two enhancements to the VAMPER model : 1) inclusion of snow as optional layers and 2) change in the timestep. The first in particular is a common issue in modeling permafrost since snow cover is a widely recognized influence on the ground thermal regime (Williams and Smith, 1989) and was not an available option in the previous VAMPER model version. To compensate for this, Kitover et al. (2013) had artificially introduced the effect of snow cover via a surface offset of + 2°C. Not only was this an assumption based on a number of previous reports and observations, but it had to be applied as an annual offset since the time step was one year. This then demonstrates the need for the other enhancement, which is a sub-annual timestep, where the seasonal changes in the ground thermal conditions can be captured, allowing for representation of both the snow cover effect and the active layer. It should be noted that additional coupling mechanisms are possible between *i*LOVECLIM components and VAMPER, which include hydrology and the carbon cycle, but are not yet implemented at this time.

In addition to these VAMPER model enhancements, two global maps were produced (geo-processed from the original maps to fit the horizontal grid of ECBilt) to be used as additional input parameters in the *i*LOVECLIM model: geothermal heat flux and lithology.

Integrating permafrost into earth system models has become of increased interest since research has acknowledged both its sensitivity to climate change along with carbon feedback implications. In fact, Koven et al. (2013) recently reported on the Coupled Model Intercomparison Project phase 5, which specifically looked at how different models represent the subsurface thermal dynamics and how well this class of models simulate permafrost and active layer depth. Despite the fact that this study introduced the variety of how different global coupled models capture permafrost, the overall

conclusion was that there is no clear ranking among their reviewed 15+ model configurations. This shows that representing permafrost in earth system models still has some challenges,which Koven et al. (2013) attribute primarily to modeling of both the atmosphere/ground energy exchange and the subsurface thermal regime. Until recently, most simulations of permafrost were calibrated for regional or local study such as Li and Koike (2003) on the Tibetan Plateau, Zhang et al. (2006) in Canada, and Nicolsky et al. (2009) in Alaska. A growing number of studies are now modeling permafrost across a global scale, namely these are from Lawrence and Slater (2005), Schaefer et al.(2011), and Dankers et al. (2011). However, it should be noted that there is a difference between coupled models which actively integrate the role of permafrost (including the thermal and/or carbon feedbacks) and models which simply look at permafrost in a post-processing perspective, meaning they are forced by the predicted temperature changes. It is the full coupling with integrated feedbacks which is of current interest but is still in the early stages since,as just mentioned, there remain challenges to accurately represent permafrost extent and active layer depths. Hence, it is the authors' ultimate goal to fully couple ECBilt and VAMPERS within iLOVECLIM, where the results of the present work serve as an important validation stage. In the sections following, the two enhancements to the VAMPER model are explained. This includes specific validation of the timestep change by comparing simulated annual active layer depths with empirical-based estimates. The ECBilt-VAMPERS semi-coupling within the *i*LOVECLIM model is then validated using a modern-day map of permafrost extent in the northern hemisphere and observed permafrost thickness and subsurface temperatures values in boreholes.

2 METHODS

2.1 VAMPER model

2.1.1. General Description

VAMPER is a 1-d permafrost model developed to estimate permafrost thickness and was designed for eventual full coupling with *i*LOVECLIM. Because it must fit a relatively coarse earth system model, it is not suitable to undergo cumbersome parameterization schemes. It is meant rather as a generalized model to simulate conceptual permafrost thickness based on the factors which most strongly dictate the subsurface thermal regime. Most notable for our purposes and discussed by Farouki (1981), these factors are mineral composition, water content, and temperature.

Other than what is specified below, construction of the VAMPER model has not changed and the methods as described in Kitover et al., (2013) still apply. In particular, these include assuming only conductive heat transfer in the subsurface, using an apparent heat capacity method for the latent heat component, and employing well-established methods for finding the temperature-dependent thermal properties of heat capacity and thermal conductivity (Farouki, 1981; Zhang et al., 2008). The subsurface is assumed to be saturated (i.e. porosity equals the water content) and there is currently no groundwater flow either horizontally or vertically between the soil layers.

2.1.2 VAMPER Model Enhancements

As compared to most permafrost modeling studies, there are few which have reproduced changes in permafrost thickness over geologic time periods. In these cases, they assume a larger timestep in their numerical simulations (usually one month or one year) (e.g., Osterkamp and Gosink, 1991; Lebret et al., 1994; Lunardini, 1995; Delisle, 1998) since they only need to force the models with the low frequency changes in air temperature or ground temperature that occur over millennia.. Since we are also interested in this timescale, we originally employed the same reasoning: relying on large-signal paleoclimatic changes (Kitover et al., 2013). However, in lightof the coupling mechanism between ECBilt and the VAMPER model, it has become clear that the VAMPER model should run on a 4-hr timestep. Doing this allows the VAMPER model to more closely follow the response timescale of the atmosphere, the subsystem to which the VAMPER model is coupled, while also allowing the numerical solution to converge since the thermal properties are temperature-dependent and hence change on every timestep. Fortunately, being that the VAMPER model is somewhat simplified, and hence flexible, this was done with some modifications to the original version. Although the original makeup of the model was validated, it has since been necessary to perform an additional verification (due to change in the timestep) while also enhancing the model with a snow layer component. *Note that the VAMPER model with the snow enhancement is referred to as the VAMPERS model. When referring to both/either versions, the "VAMPER(S)" term is used.*

Timestep

To illustrate the difference between applying the same annual average temperature forcing but with two different timesteps (4-hr vs. yearly), a sensitivity test was performed (**Fig. 1a**). To generate the sub-daily surface temperature forcing (4 hours), a year-long temperature time-series was calculated using a standard sine function with constant amplitude 20°C and average annual temperature of -6 °C (hereafter referred to as sensitivity run 1 or "sr1"), resulting in an annual range of temperatures between -26 °C and 14°C. Therefore, the case with a yearly timestep, called "sr2", simply used -6 °C as the constant forcing. Besides the change in timestep and corresponding surface temperature forcing, the thermal conductivity and heat capacity values were also allowed to differ since these variables are temperature-dependent (**Fig. 1b**). However, heat flux and porosity parameter settings were the same in both model runs. Each experiment was run until approximate equilibrium was reached under the same constant (respective) forcing. We consider equilibrium to be when the geothermal heat flux is approximately equal to the ground heat flux (what goes in = what goes out). Comparing the final depth-temperature profiles between sr1 and sr2 shows a shift in the equilibrium depth-temperature profile where using an annual timestep underestimates permafrost thickness by approximately 50 meters (**Fig. 1a**). This difference is attributed to occurrence of the thermal offset within the active layer in sr1 (**Fig. 1b**), whereas sr2 cannot exhibit such seasonal phenomena. Since VAMPER is a simple model (absence of vegetation, organics, an unsaturated subsurface, or temporally varying water content) we can easily attribute the thermal offset to seasonal differences in thermal conductivity, whereas the thermal conductivity of ice is four times that of unfrozen water and therefore the freezing front is propagated more effectively than the warming front. This difference causes the mean annual subsurface

temperature within the active layer to be gradually colder with depth. The offset is visible in the mean annual depth-temperature profile within the top meter of Figure 1b.

Active Layer

Since a sub-daily time step is used, the VAMPER model as expected produces an active layer. Most dynamical permafrost models that simulate near-surface behavior configure the parameter settings to specifically match locally observed data. Common parameterizations include organic and mineral layer thicknesses, which give soil properties such as porosity and bulk density, and unfrozen water content characteristics. Examples of these site-specific studies are numerous (e.g., Romanovsky and Osterkamp, 2000; Buteau et al., 2004, Ling and Zhang, 2004; Zhang et al., 2008; Nicolsky et al., 2009). Since VAMPER is not parameterized to capture site-specific behavior, it is challenging to assess the ability of the model to simulate active layer dynamics. Fortunately, there is a common calculation called the Stefan equation, used originally in engineering applications (Fox et al., 1992), to estimate the thickness of the active layer when the amount of energy input and thermal characteristics are known. From French (2007), the Stefan equation is defined as

$$AL = \sqrt{2\sigma k_{mw}/Q_i} \quad (1)$$

where *AL* (m) is the thickness of the active layer, σ is the cumulative thawing index (average ground surface temperature (°C) during the thaw season times the duration of thaw season (*s*)), and k_{mw} is the thermal conductivity of unfrozen soil (W (m K)$^{-1}$). Q_i (J m^{-3}) is defined further as

$$Q_i = L\rho_m(W - W_u) \quad (2)$$

where L is the latent heat of fusion, ρ_m is the dry density of the soil (kg m^{-3}), W is the total moisture content , and W_u is the unfrozen water content . **Table 1** gives the constant variable values applied in the Stefan Equation, which are the same values used in a comparable run for the VAMPER model

Under different forcings as a function of both average annual ground surface temperature and annual amplitude, the VAMPER model's active layer thickness versus results using the Stefan Equation are shown in **Table 2**. It is clear when comparing the empirically-based results with the series of simulations, that the VAMPER model does a suitable job of reproducing annual active layer thickness.

Snowpack parameterization

An additional option to the VAMPER model is the ability to extend the heat conduction model into the snowpack when present. Prior to this, the surface offset, as illustrated in Smith and Riseborough (2002), could not be applied in the VAMPER model.

The VAMPERS model uses snow water equivalent (*swe*) values (m) with corresponding density to compute snow thickness layers. Snow water equivalent is the depth of water that would result from the complete melting of snow. The precipitation simulated in ECBilt is computed from the precipitable water of the first atmospheric layer (Goosse et al., 2010). When the air temperature is below 0 °C, the precipitation is assumed to be snow. However, this 'snow' is only assumed to be frozen water, meaning

it lacks any quantifiable properties besides the actual precipitation amount, and as such is directly considered the *swe* value. As a result, there is an additional set of necessary functions when coupled with VAMPERS to transfer ECBilt s*we* values into a snowpack thickness (Z) at time *t*:

$$Z^t = \rho_w \, swe^t / \rho_s^t \tag{3}$$

where ρ_w is water density and ρ_s snow density (Lynch-Stieglitz, 1994). The total snow density is determined as a combination of old snow (expressed as swe^{t-1} from the previous timestep) and freshly fallen snow at current timestep (expressed as swe^{fr}) :

$$\rho_s^t = \left(swe^{t-1} \, \rho_s^{t-1} + swe^{fr} \, \rho_{fr} \right) \Big/ swe^t \tag{4}$$

$$swe^t = swe^{t-1} + swe^{fr} \tag{5}$$

where ρ_{fr} is the density of fresh snow (150 kg m^{-3}).

There is snowpack metamorphism that occurs from a number of different processes. Notably, Dingman (2002) distinguishes these as gravitational settling, destructive, constructive, and melt. However, as these different changes occur at highly varying rates and under localized conditions (aspect, slope, vegetation cover), it is nearly impossible to incorporate such processes in an Earth System Model of Intermediate Complexity (EMIC) such as *i*LOVECLIM. On the other hand, a snowpack always undergoes densification over time and this effect should somehow be applied to the modeled snowpack. Therefore, we apply to the total snow density an empirical densification function due to mechanical compaction. The maximum allowable density is 500 kg m^{-3}, which typically cannot hold any more liquid water (Dingman, 2002). The compaction equation used (e.g. Pitman et al.,1991; Lynch-Stieglitz, 1994;) is as follows:

$$\rho_s^t = \rho_s^{t-1} + \left(0.5 \times 10^7 \rho_s^{t-1} \, g \, N \exp\left[14.643 - \frac{4000}{\min(T+273.16 \, , 273.16)} - 0.02 \rho_s^{t-1} \right] \right) \Delta t \tag{6}$$

where *g* is gravity (9.82 m s^{-2}), *N* (kg) is the mass of half the snowpack, *T* (°C) is the temperature of the snowpack (the average temperature of the snow layer temperatures from the previous timestep), and Δt is the timestep (*s*).

Three snow layers are then discretized from the total snow thickness, depending on whether it is above or below 0.2 m, as outlined in Lynch-Stieglitz (1994). Thermal properties are then calculated for each snow layer based on empirical formulas :

$$K_s = 2.9 \, {\rho_s}^2 \qquad \text{(Goodrich, 1982)} \tag{7}$$

$$C_S = 1.9 \times 10^6 \rho_s / \rho_f \qquad \text{(Verseghy, 1991)} \tag{8}$$

where K_s is the snow thermal conductivity and C_s is the snow heat capacity, and ρ_f is the density of ice (920 kg m^{-3}). All three snow layer are subject to the same processes and simply depend on temperature, time, and thickness for their respective deformation and/or melting.

The following is a stepped description of the snow algorithm for the ECBilt-VAMPERS semi-coupling:

1. Calculate new snow density, Eq. (4) and Eq. (5), using any freshly fallen snow and old snow.
2. Apply compaction function, Eq. (6), to already existing snowpack
3. Calculate total snow thickness using Eq. (3).
4. Discretize the individual layer thicknesses based on total snow thickness.
5. Calculate thermal properties for each layer (Eq. (7) and Eq. (8)).
6. Use snow thicknesses and corresponding thermal properties as additional layers in the VAMPERS model.

2.2 *i*LOVECLIM v 1.0

2.2.1 General Description

*i*LOVECLIM is a "code-fork" of LOVECLIM 1.2 (Goosse et al., 2010), both which belong to a class of climate models called EMICs (Claussen et al., 2002). This type of model, as summarized by Weber (2010), "describes the dynamics of the atmosphere and/or ocean in less detail than conventional General Circulation Models". This simplification reduces computation time, thus making EMICs suitable for simulations on millennial timescales, incorporating the components with slow feedback effects, such as icesheets, vegetation, and permafrost. Different versions of LOVECLIM have successfully simulated past climates including the LGM (Roche et al., 2007), the Holocene (Renssen et al., 2005, 2009), and the last millennium (Goosse et al., 2005). Although there exist some different developments between *i*LOVECLIM and the LOVECLIM versions, both consist of the following coupled earth system components: the atmosphere (ECBilt), the ocean (CLIO), and vegetation (VECODE) (**Fig. 2**). Each component was originally developed separately and the reader is referred to Goosse et al., 2010 for a detailed description. Furthermore, *i*LOVECLIM more recently includes other optional components including an ice-sheet model (Roche et al., 2014) and a stable water isotopes scheme (Roche, 2013).

2.2.2 ECBilt-VAMPER(S) Coupling Description

The atmospheric component, ECBilt (Opsteegh et al., 1998), which the VAMPER(S) model is specifically coupled to, runs on a spectral grid with a triangular truncation (T21). This translates to a horizontal grid with a resolution of approximately 5.6 ° lat x 5.6 ° lon. The ECBilt-VAMPER(S) semi-coupling is done via the air surface temperature from ECBilt at each timestep (4 hours), which the VAMPER(S) model uses as the ground temperature forcing. The air surface temperature is calculated within ECBilt as a function of the heat balance equation where the major heat fluxes across the air/surface interface are incorporated: sensible heat flux, latent heat flux, shortwave radiation, and longwave radiation. The air surface temperature is only communicated to the VAMPER(S) model when the respective grid cell is classified as land with no overlying icesheet (i.e. Greenland/Antarctica at present day). Since the VAMPER(S) model ground surface temperature is taken to be the ECBilt air surface temperature, there is no surface offset effect except when there is a snowpack. In this case, the snow surface temperature is taken to be the air surface temperature . This means the VAMPERS model ground temperature forcing is buffered via the three snowpack layers as discussed in Sect. 2.1.2. Using the ground surface

temperature forcing, the VAMPER(S) model then computes the subsurface temperature profile. This calculation, via the implicitly solved heat equation with phase change capability, is fully described in Kitover et al. (2013). As VAMPER is a 1-D model, there is no lateral energy (heat/water) transfer between adjacent grid cells in the subsurface. Permafrost thickness is determined at an annual timestep using a computed average annual temperature profile, where any depth below or equal to 0°C is considered permafrost. Although there is a freezing point depression which may occur as a result of the local pressure or dissolved salts, we are consistent with the common thermal definition of permafrost from the International Permafrost Association: "ground (soil or rock and included ice or organic material) that remains at or below 0°C for at least two consecutive years".

The land surface of ECBilt consists of a single "layer" which represents a volumetric storage capacity to generate surface runoff when full. This system is often referred to as a bucket model in previous text. As of currently, this bucket model, which is the surface hydrology in iLOVECLIM, is not coupled to VAMPERS. It would be a sensible next step to connect the active layer with this bucket model

The results presented in this current work is only a function of performing semi-coupled experiments and are means as an intermediary step to a fully coupled model in order to validate both VAMPERS and its ability to model permafrost extent and thickness. In future experiments, VAMPERS will be fully coupled to ECBilt. In this case then, at the end of each timestep, VAMPER(S) would calculate the ground heat flux and return this value to ECBilt (Fig. 3) as one of the variable terms in the surface heat balance equation (among the other fluxes such as sensible heat flux, latent heat flux, etc.) , which in turn would be used to obtain the air surface temperature for the next time step.. The equations for this full coupling will be described in a future publication.

2.2.3 Geothermal Heat Flux

The VAMPER(S) model requires a geothermal heat flux as the lower surface boundary. In Kitover et al. (2013), a sensitivity analysis was performed to look at the equilibrium permafrost thickness as a result of varying the geothermal heat flux and found that thickness can increase by about 70 m with every decrease in flux of 10 mW m^{-2}. To obtain the geothermal heat flux for every cell in the ECBilt grid, we

used the recent publication of Davies (2013) who determined the median of heat flux estimates per approximately 2° x 2° latitude-longitude grid based on a combination of actual measurements, modeling, and correlation assumptions. However, due to the mismatch of grid resolutions between Davies (2013) and ECBilt, we determined for each ECBilt grid cell, a simple area-weighted average of the Davies (2013) estimates. In other words, each of the Davies grid cells was assigned a weighing factor based on the percentage of overlap with the ECBilt cells. Below is the original map from Davies (2013) and the averaged map applied in the *i*LOVECLIM experiments (**Fig. 4**). A preliminary sensitivity analysis between applying the geothermal heat flux map and applying the continental global average (approx. 60 mW m^{-2}) showed no noticeable difference in permafrost distribution. This result is different, however, than the noticeable sensitivity of geothermal heat flux on permafrost depth.

2.2.4 Porosity

Another variable needed to run the VAMPER(S) model is the porosity values throughout depth, which in these experiments is down to 3000 meters deep. In previous VAMPER studies (Kitover et al., 2013; Kitover et al., 2012), it was always assumed that the land subsurface was sedimentary rock, with a porosity of 0.3, 0.4, or 0.5. However, as shown in Kitover et al. (2013), the porosity, or water content, has a noticeable effect on equilibrium permafrost thickness. That sensitivity test showed about a 50 m difference in permafrost thickness when the porosity values (assuming a saturated subsurface) ranged between 0.3 and 0.5. Therefore, to both narrow our assumptions regarding the subsurface but still maintain the simplification necessary for the coarse horizontal grid, an additional lithological classification scheme was created as an additional VAMPER(S) model parameter. Using the recently published Global Lithological Map Database (GLiM) from Hartmann and Moosdorf (2012), their original seven categories were reclassified into 'Bedrock (Bed)' , (e.g., granitic and metamorphic rock), and 'Sedimentary (Sed)' (e.g., sandstone, limestone) (**Table 3, Fig. 5**). In the case of 'Bed', the subsurface would presumably be quite consolidated/compressed, resulting in a low water content (Almén et al., 1986; Gleeson et al., 2014). 'Bed' was thus assigned a low porosity of 0.1, which based on sources that showed depth profiles of bedrock sites (Schild et al., 2001; Nováková et al., 2012), stayed constant with depth. On the other hand, similar to the case studies from Kitover et al. (2013), a depth porosity function from Athy (1930) was applied for the 'Sed' class, where the surface porosity (Φ) was assumed to be 0.40 and a decay constant (4×10^{-4}) in the exponential equation, representing the average for sandy textured soil. Similar to application of the geothermal heat flux map, a preliminary sensitivity analysis between applying the lithology map and applying a constant value (0.4) throughout the globe showed only marginal differences in permafrost distribution. This result is different, however, than the higher sensitivity of porosity on permafrost depth.

3 Validation of preindustrial permafrost thickness distribution

3.1 Experimental Setup

The model experiments are performed over the whole globe semi-coupled, which means that ECBilt passes the air surface temperature values to the VAMPER(S) model (right side of **Fig. 3**) but no data is returned to ECBilt (left side of **Fig. 3**), leaving the climate unaffected from permafrost or changes in permafrost. This configuration, therefore, allows only the examination of the *i*LOVECLIM model to reproduce current permafrost extent and depths as function of the currently established climate of the *i*LOVECLIM model. Two different model runs were made: one without the snow enhancement or any imposed surface offset (ECBilt-VAMPER coupling) and one with the snow enhancement (ECBilt-VAMPERS coupling). These two are first compared in sect. 3.2.1 of the Results & Discussion below.

Because permafrost has a very slow thermal response (Lunardini, 1995) as compared to other components in *i*LOVECLIM, VAMPER(S) is not run in a continuous (semi) coupling with ECBilt. Rather, they are run together continuously for 100 years and then VAMPER(S) runs offline for 900 years using the ECBilt average air surface temperature of the previous 100 years as the forcing. This asynchronous cycle is repeated for thousands of years until approximate equilibrium between the ECBilt temperatures

and the VAMPER(S) model is reached. This scheme is illustrated in **Fig. 6** (adapted from a similar figure in McGuffie and Henderson-Sellers (2005)). Equilibrium was determined when the lower boundary heat flux approximately matches the annual average ground surface heat flux. This is also of course when the permafrost thickness is stable. Although the model approaches a steady state through the subsurface depth, we acknowledge that in reality, some of the permafrost regions are not at equilibrium since they are responding to recent warming.

3.2 Results and Discussion

In order to verify the performance of the ECBilt-VAMPER(S) coupling within *i*LOVECLIM, a series of equilibrium experiments were performed for the preindustrial (PI) climate (~ 1750 AD). For comparative purposes, we assume the PI state of permafrost is similar enough to the current state of permafrost that we used modern-day data to validate against the PI simulations. The simulated areal extent was compared to present-day extent using the well-known "Circumarctic Map of Permafrost and Ground-Ice Conditions" (Brown et al., 2014). Unlike the model validation done by Lawrence and Slater (2005), and then subsequently critiqued by Burn and Nelson (2006), our simulations attempt to capture the extent of both continuous and discontinuous permafrost. In addition, available borehole data, for sites within the arctic/subarctic, were used to evaluate the simulated thicknesses. Therefore, there are essentially two types of validation approaches: 1) horizontal (spatial extent) and 2) permafrost depth.

3.2.1 Permafrost Distribution Validation

The first validation demonstrates how well the *i*LOVECLIM model reproduces the modern-day permafrost extent by overlaying the simulated results on the map from Brown et al. 2014.

Using a comparison between the different couplings (**Fig. 7**), it is clear that the experiment where the ECBilt- VAMPER semi-coupling (no snowoption and no imposed surface offset) is used overestimates permafrost extent while employing the ECBilt -VAMPER**S** version underestimates it. This swing of inaccuracy is at least partially due to simply attempting to match results from a low resolution grid to spatial coverage of much higher resolution. In addition, we expect some inaccuracy since we cannot parameterize the snowpack characteristics and more importantly, the nature of the snowmelt. As opposed to our generalized approach described earlier, high resolution snowmelt models are fitted to observational data by analyzing, for example, the physics of accumulation, areal distribution, and snow-soil interactions. Therefore, it is arguable from **Fig. 7** and the recognized discrepancies in generalizing snow model details, whether the better option is to include snowpack in VAMPERS or not. However, as long as the VAMPERS model is doing a reasonable job, we contend it is a better option over merely applying artificial offsets or assuming none at all since snow plays a critical role in the ground thermal conditions and should be represented. Further, with the snow optiont, changing precipitation patterns that are often the byproduct of a shifting climate would otherwise have no effect on the subsurface thermal conditions. In other words, the role of snow cover is likely more noticeable in using the ECBilt-VAMPERS coupling when doing transient experiments. From this point forward, all analysis is done using results from the ECBilt-VAMPERS coupling (i.e. *with* the snow option).

Employing the snow option in the ECBilt-VAMPERS coupling produces the surface offset that would naturally occur from the snowpack (Goodrich, 1982; Smith and Riseborough, 2002). The simulated global distribution of this offset is shown in **Fig. 8**. It is determined by calculating the difference between the mean annual ground temperature (MAGT) using the ECBilt-VAMPERS coupling and the MAGT using the ECBilt-VAMPER coupling (no snow option and no imposed offset). Although the maximum mean annual surface offset is about 12 °C, the average among all the grid cells that had snow cover is about 2.7 C, which is close to our original applied offset of 2 °C in Kitover et al., (2013). Values between 1 °C and 6 °C were reported early on by Gold and Lachenbruch (1973). Monitoring studies of the air-ground temperature relationship also fall within this range e.g., Beltrami and Kellman (2003), Bartlett et al., (2005), Grundstein et al., (2005), Zhang (2005). However, larger values of 10 °C have been recorded in Alaska (Lawrence and Slater, 2010).

In addition to the offset imposed by incorporation of a snowpack, there are a number of factors which have been commonly recognized in affecting the surface offset and hence should be part of the air-ground coupling. Depending on the scale of interest, the magnitude of these can vary but a standard list includes surface organic layer, vegetation, overlying water bodies, and wind. It should be recognized that within ECBilt, some of these factors are reflected in the air surface temperature (notably wind and a simplified vegetation scheme) but the others are absent. In addition, coupling the ECBilt surface hydrology to the groundwater storage would affect both the ground thermal regime and hydrological regime. In the first case, subsurface water content affects the thermal properties of the soil. In particular, the conductivity of organics have high variation seasonally. In the second instance, frozen ground is impermeable, allowing little or no subsurface water storage, in turn affecting runoff flowrates and timing.

The permafrost distribution simulated by *i*LOVECLIM can be matched against results from a study comparing a suite of earth system models, namely the Coupled Model Intercomparison Project phase 5 (CMIP5) (Koven et al., 2013). This report gives the simulated preindustrial permafrost areas under a number of different earth system climate models and configurations. Compared to the results from *i*LOVECLIM, some of the other models' simulated permafrost distributions cover more area while some cover less. The maximum is reported as 28.6 x 10^6 km^2 and minimum 2.7 x 10^6 km^2. The simulation by *i*LOVECLIM yields approximately 20.3 x 10^6 km^2 . This is a reasonably comparable estimate considering almost 80 % (14/18) of the model area extents from Koven et al. (2012) fall within 40% (12 – 28 x 10^6 km^2) of our model estimates. According to discussion by Koven et al., (2012), most of the variation seen among the compared earth system models is primarily attributed to the subsurface modeling techniques, such as water content, using a latent heat term, and differing soil thermal conductivities. Secondary causes are attributed to the air-ground coupling such as incorporation of organics and a snowpack (bulk or multilayer). These conclusions are not different from our own study in that 1) snowpack plays a marked role in permafrost modeling and inclusion/exclusion will impact the results, 2) the air-ground coupling is also a source of potential mismatch (discussed further in section 3.2.2).

3.2.2 Permafrost Thickness Validation

The second validation examines the simulated depth of permafrost using borehole data taken from the Global Terrestrial Network for Permafrost (GTN-P; www.gtnp.org). The scatterplot (**Fig. 9**) shows all the observed borehole measurements mapped in **Fig. 10** versus the corresponding permafrost depth

simulated by *i*LOVECLIM. It is clear that there is a larger divergence between modeled and observed depths for the deeper permafrost than for the more shallow observations, where some points are relatively overestimated (> 300 m) and some very underestimated (>700 m). There are a number of reasons to explain the mismatch, which can occur in the borehole data and/or the model data. The first explanation is that the borehole estimates have a given range of uncertainty since measurement techniques and subsequent interpretations are subject to error. Osterkamp and Payne (1981) describe in detail potential errors associated with the freezing point depression, thermal disturbance, and lithology.

The second cause is that we assumed implicitly that the observed permafrost depths are at equilibrium with the current (or PI; preindustrial) climate state. This is probably why there is a striking mismatch at the central Siberian site (66° 26’ 2” N, 112° 26’ 5” E) (point 1, **Fig. 9**), where the permafrost is estimated from the borehole data to be 1000 m thick while the corresponding modeled value is only about 375 m. It is very likely that, like much of the Siberian permafrost, this permafrost developed from the preceding glacial period (Kondratjeva et l.,1993). Another example concerns western Siberia, (points 2 through 4, **Fig. 9**), which is an area well documented for having relict permafrost (Zemtsov and Shamakhov, 1992; Ananjeva et al., 2003). It is also identified in the “Circumarctic Map of Permafrost and Ground-Ice Conditions” (Brown et al., 2014) and “The Last Permafrost Maximum (LPM) map of the Northern Hemisphere” (Vandenberghe et al., 2014). But it should be noted that not all the relict permafrost in western Siberia is of late Pleistocene origin and may be from earlier cold stages (Zemtsov and Shamakhov, 1992; French, 2007).

Another reason for some discrepancies between modeled and observed data is that high-resolution features in the landscape and topography cannot be captured by *i*LOVECLIM due to the limited spatial resolution and hence, a small set of model parameters. Such factors as vegetation and organic layer, which can vary due to local topography and micro-climatic conditions, have been shown to affect the active layer and ground thermal regime (Shur and Yorgenson, 2007; Fukui et al., 2008; Lewkowicz et al., 2011; Wang et al., 2014). Consequently, given a specific borehole site, some discrepancy in the permafrost thickness estimate will likely occur between our simplified interpretation and that which results from including more complex and local interactions. It is possible, for example, that the observed value for point 5 (720 m) is a function of higher elevation since it is from a borehole site in the Russia Highlands but this relatively local elevation effect may not be a strong enough signal in the *i*LOVECLIM surface temperatures, and hence is underestimated.

The other outlying points (points 6 and 7, **Fig. 9**) occur in Canada but as opposed to the relict sites as mentioned above, *i*LOVECLIM overestimates the permafrost thickness quite noticeably. These discrepancies, both occurring at high latitudes of 80 °N and 76 °N , reveal that VAMPERS is probably not reproducing the subsurface temperatures well for this area. For example, a report for the specific borehole (Gemini E-10; point 6, **Fig. 9**) calculated the geothermal gradient to be approximately 0.04 °C/m (Kutasov and Eppelbaum, 2009) whereas our model result for the corresponding grid space found a gradient of approximately 0.03 °C/m. Although this difference may seem small, it hints at either a necessary increase in the averaged geothermal heat flux used in the model or a change in the

subsurface thermal properties (increase in thermal conductivity), which could be altered by an adjustment in the VAMPERS water content.

3.2.3 Climate analysis

Finally, the remaining possibility to explain inaccuracies between the modeled results and the observed results (both in reproducing spatial extent and permafrost thickness) is the *i*LOVECLIM climate. Results of the VAMPER model, above all other parameter settings, are most dependent on the mean annual ground surface temperature, as shown in the sensitivity study from Kitover et al. (2013), so if there exists biases or discrepancies within the forcing, it will be reflected in the semi-coupled output. For this portion of our analysis, we took observed mean annual ground temperature (MAGT) measurements from again the GTN-P (IPY Thermal State of Permafrost Snapshot, IPA 2010) . As a result, we composed a 1:1 comparison between the observed MAGT and the corresponding simulated MAGT at the same approximate depth and location (**Fig. 11**). **Figure 12** shows a map of the selected GTN-P measurements. All the temperature comparisons are within the top thirty meters of the subsurface and therefore reflect the present or very recent climate as opposed to the deeper temperatures (i.e., > 150 m) that, depending on subsurface thermal diffusivity and surface temperature perturbations, can reflect historical temperatures of at least one hundred years ago (Huang et al., 2000) and up to tens of thousands of years (Ter Voorde et al., 2014).

Overall, **Fig. 11** illustrates that ECBilt-VAMPERS does a reasonable job of predicting shallow subsurface temperatures since a majority of the points fall near the 1:1 line. This result, therefore, supports the notion that the preindustrial climate is well represented by *i*LOVECLIM. The points of Kazakhstan and Mongolia, and a few others in Russia, have a warm bias in the forcing (simulated is warmer than observed), which is probably due to an inaccurate representation of elevation temperature changes in *i*LOVECLIM, since many of those sites are at elevations above 1000 m. Even applying the lapse rate for a standard profile (6.5 C / km; McGuffie & Henderson-Sellers, 2013) would presumably make a significant difference on the depth since earlier sensitivity tests (Kitover et al., 2013) showed an average 55 m increase in equilibrium permafrost depth for every 1 °C colder. On the other hand, many of the other points show that predicted subsurface temperatures are on average a few degrees colder than the observed, leading to the most obvious conclusion that a cold bias exists in the *i*LOVECLIM climate. Although the cold bias, most obvious for Canada and Alaska, is congruent to the overestimation in permafrost thickness evident from the geographic breakdown illustrated in **Fig. 10**, it has not previously been substantiated in former analyses of LOVECLIM or *i*LOVECLIM so it is more likely that such a discrepancy is due to the air-ground coupling as opposed to simply the air surface temperature forcing. Indeed, there a number of other (sub)surface processes not included in the current ECBilt-VAMPERS coupling which may reduce the apparent cold bias. These effects primarily alter the seasonal behavior of the thermal diffusivity in the subsurface and have been well-documented in observational studies (Williams and Burn, 1996; Woo and Xia, 1996; Fukui et al., 2008). Smith and Riseborough (2002) simplified these mechanisms intothe surface offset (air to ground surface) and the thermal offset (ground surface to top of the permafrost). Due to minimal parameterization of the VAMPERS model, these offsets may be somewhat overlooked.

For now, the average range of error between observed and predicted is about 2.6 °C. Given that the comparisons are between point-based observations and large grid cell values, meant to represent a relatively large surface area, some variability is expected to occur.

4 Next Steps

The results of this paper demonstrate the ability of ECBilt-VAMPERS semi-coupling within *i*LOVECLIM to model current permafrost distribution and thickness. The next step is to analyze the feedback that permafrost changes have on the climate. This has been of particular interest of the last decade since it is clear that specific feedbacks exists, most notably the release of locked-up carbon in the atmosphere as permafrost degrades (Anisimov, 2007). The initial method behind a full coupling would be to integrate the additional coupling mechanisms, shown in **Fig. 3,** and reanalyze the equilibrium results (since a full coupling would likely lead to an altered equilibrium permafrost state). In addition, the feedback effects would be most visible during millennial-scale transient climate shifts, when major permafrost degradation and/or disappearance is likely to occur.

5 Conclusions

Enhancements have been made to the VAMPER model to make possible the first version of the ECBilt-VAMPERS semi-coupling. The change in timestep to 4 hours was necessary to match the timestep of ECBilt and allow the seasonal effects, notably snow cover and the active layer, to be reflected in the simulation of permafrost. The predicted annual active layer from the stand-alone VAMPER model, under different temperature forcings, compare well with results from the Stefan equation. We also described the snow option, which introduces the thermal insulation effects and changes in the thermal properties of snow over time due to varying snow densities. In addition, we developed two new maps: geothermal heat flux and porosity. Incorporating these parameters at a global scale was an important step in improving the horizontal spatial variability of permafrost thickness/distribution while also maintaining the simplicity and efficiency of ECBilt-VAMPERS.

Using a semi-coupled ECBilt-VAMPER(S) component within *i*LOVECLIM, equilibrium experiments for the PI climate show that when the snow component is included in the VAMPER model, the permafrost extent is noticeably reduced while the average offset of 2.7 °C is comparable to previous reports. We then compared both permafrost thickness estimates and subsurface temperatures to corresponding observed values. Considering that we are comparing point measurements to gridcell-based values, the simulations are quite reasonable. There are some discussion points around the most obvious discrepancies. One is that the relatively coarse horizontal ECBilt grid will never perfectly match the sensitivity of permafrost occurrence and depth due to local factors. This is also the case in the air-land temperature coupling, where some of the local effects will simply not be present in an EMIC. Similarly, when *i*LOVECLIM does not accurately represent the environmental lapse rate in areas of higher elevation , the occurrence of permafrost in these areas are overlooked by the VAMPERS model. Finally,

some of the observed permafrost depths are not a function of the present (PI) climate, but rather a relict presence from previous cold periods. Therefore, when comparing measured to simulated results, some underestimations expectedly occurred. It is only with millennial-scale transient *i*LOVECLIM model runs that we can simulate, for example in areas of West Siberia, how permafrost evolved over periods of major climate change.

6 Code availability

The *i*LOVECLIM (version 1.0) source code is based on the LOVECLIM model version 1.2 whose code is accessible at http://www.elic.ucl.ac.be/modx/elic/index.php?id=289. The developments on the *i*LOVECLIM and VAMPER(S) source code are hosted at https://forge.ipsl.jussieu.fr/ludus but are not publicly available due copyright restrictions. Access can be granted on demand by request to D. M. Roche (didier.roche@lsce.ipsl.fr).

References

Almén, K., Andersson, J. , Carlsson, L., Hansson, K., and Larsson, N.: Hydraulic testing in crystalline rock. A comparative study of single-hole test methods, Swedish Nuclear Fuel and Management Company, Uppsala, Sweden, SKB Technical Report 86-27, 190 pp., 1986.

Ananjeva (Malkova), G.V., Melnikov, E.S., and Ponomareva, O.E.: Relict permafrost in the central part of western Siberia, in: Proceedings of 8th International Conference on Permafrost, Zurich, Switzerland, 5-8, 2003.

Anisimov, O.A.: Potential feedback of thawing permafrost to the global climate system through methane emission, Environ. Res. Lett., 2, 045016, doi:10.1088/1748-9326/2/4/045016, 2007.

Athy, L.F.: Density, porosity, and compaction of sedimentary rocks, Am. Assoc. Petrol. Geol. Bull, 14, 1-24, 1930.

Bartlett, M.G., Chapman, D.S., and Harris, R.N.: Snow effect on North American ground temperature 1950-2002, J. Geophy. Res., 110, F03008, doi: 10.1029/2005JF000293, 2005.

Beltrami, H. and Kellman, L.: An examination of short- and long-term air–ground temperature coupling, Global Planet. Change, 38, 291-303, 2003.

Burn, C.R and Nelson, F.E.: Comment on ‘‘A projection of severe near-surface permafrost degradation during the 21st century’’ by David M. Lawrence and Andrew G. Slater, Geophy. Res. Lett., 33, L21503, doi:10.1029/2006GL027077, 2006.

Buteau, S., Fortier, R., Delisle, G., and Allard, M.: Numerical simulation of the impacts of climate warming on a permafrost mound, Permafrost Periglac., 15, 41-57, 2004.

Brouchkov, A., Fukuda, M., Iwahana, G., Kobayashi, Y., and Konstantinov, P.: Thermal conductivity of soils in the active layer of eastern Siberia, Permafrost Periglac., 16, 217-222, 2005.

Brown, J., Ferrians, O., Heginbottom, J.A., and Melnikov, E.: Circum-Arctic Map of Permafrost and Ground-Ice Conditions, National Snow and Ice Data Center, Boulder, CO, 2014.

Claussen, M., Mysak, L.A., Weaver, A.J, Crucifix, M., Fichefet, T., Loutre, M.-F., Weber, S.L., Alcamo, J., Alexeev, V.A., Berger, A., Calov, R., Ganopolski, A., Goosse, H., Lohmann, G., Lunkeit, F., Mokhov, I.I., Petoukhov, V., Stone, P., and Wang, Z.: Earth system models of intermediate complexity: closing the gap in the spectrum of climate system models, Clim. Dynam., 18, 579-186, 2002.

Dankers, R., Burke, E.J. and Price J.: Simulation of permafrost and seasonal thaw depth in the JULES land surface scheme, The Cryosphere, 5, 773-790.

Davies, J.H.: Global map of solid earth heat flow, Geochem. Geophy. Geosy., 14, 4608-4622, doi: 10.1002/ggge.20271, 2013.

Delisle, G.: Numerical simulation of permafrost growth and decay, J. Quaternary Sci., 13, 325-333, 1998.

Dingman, S.L.: Physical Hydrology, Second Edition, Prentice Hall, Upper Saddle River, N.J., 2002.

Farouki, O.T.: Thermal properties of soils, Cold Regions Research and Engineering Laboratory, Hannover, N.H., CRREL Report 81-1, 136 pp., 1981.

Fox, J.D.: Incorporating freeze-thaw calculations into a water balance model, Water Resour. Res., 38, 2229-2244, 1992.

French, H.M.: The Periglacial Environment, Third Edition, Jon Wiley & Sons Ltd, West Sussex, England, 2007.

Fukui, K., Sone, T., Yamagata, K., Otsuki, Y., Sawada, Y., Vetrova, V., and Vyatkina, M.: Relationships between permafrost distribution and surface organic layers near Esso, Central Kamchatka, Russian Far East, Permafrost Periglac., 19, 85-92, doi: 10.1002/ppp.606, 2008.

Gleeson, T., Moosdorf, N., Hartmann, J., and van Beek, L. P. H.: A glimpse beneath earth's surface: GLobal HYdrogeology MaPS (GLHYMPS) of permeability and porosity, Geophys. Res. Lett., 41, 2014GL059856, doi:10.1002/2014gl059856, 2014.

Gold, L.W. and Lachenbruch, A.H.: Thermal conditions in permafrost - a review of North American literature, in: Permafrost: The North American Contribution to the Second International Conference, Yakustsk, USSR, 13-28 July 1973, 3-23, 1973.

Goodrich, L.E.: The influence of snow cover on the ground thermal regime, Can. Geotech. J., 19, 421-432, 1982.

Goosse, H., Renssen, H., Timmermann, A., and Bradley, R. S.: Internal and forced climate variability during the last millennium: a model-data comparison using ensemble simulations, Quaternary Sci. Rev., 24, 1345–1360, 2005.

Goosse, H., Brovkin, V., Fichefet, T., Haarsma, R., Huybrechts, P., Jongma, J., Mouchet, A., Selten, F., Barriat, P.Y., Campin, J., Deleersnijder, E., Driesschaert, E., Goelzer, H., Janssens, I., Loutre, M., Morales Maqueda, M.A., Opsteegh, T., Mathieu, P., Munhoven, G., Pettersson, E.J., Renssen, H., Roche, D.M., Schaeffer, M., Tartinville, B., Timmermann, A., and Weber, S.L: Description of the earth system model of intermediate complexity LOVECLIM version 1.2, Geosci. Model Dev., 3, 603-633, DOI: 10.5194/gmd-3-603-2010, 2010.

Grundstein, A., Todhunter, P., and Mote, T.: Snowpack control over the thermal offset of air and soil temperatures in eastern North Dakota, Geophy. Res. Lett., 32, L08503, doi:10.1029/2005GL022532, 2005.

Hartmann, J. and Moosdorf, N.: The new global lithological map database GLiM: A representation of rock properties at the Earth surface, Geochem. Geophy. Geosy., 13, Q12004, doi:10.1029/2012GC004370, 2012.

Huang, S., Pollack, H.N., and Shen, P.: Temperature trends over the past five centuries reconstructed from borehole temperatures, Nature, 403, 756-758, 2000.

Kitover, D.C., Renssen, H., Vandenberghe, J., and van Balen, R.T.: Modeling permafrost response of the last glacial termination: first results of the VAMPER model, in: Proceedings of the 10th International Conference on Permafrost, Salekhard, Russia, 25-29 June 2012, 209-214, 2012.

Kitover, D.C., van Balen, R.T., Roche, D.M., Vandenberghe, J., and Renssen, H.: New estimates of permafrost evolution during the last 21 k years in Eurasia using numerical modelling, Permafrost Periglac., 24, 286-303, 2013.

Kondratjeva, K.A., Khrutzky, S.F., and Romanovsky, N.N.: Changes in the extent of permafrost during the late Quaternary period in the territory of the former Soviet Union, Permafrost Periglac., 4, 113-119, 1993.

Koven, C.D., Riley, W.J., and Stern, A.: Analysis of permafrost thermal dynamics and response to climate change in the CMIP5 earth system models, Journal of Climate, 26, 1877-1900, doi: 10.1175/JCLI-D-12-00228.1, 2013.

Kutasov, I.M. and Eppelbaum, L.V.: Estimation of geothermal gradients from single temperature log-field cases, J. Geophys. Eng., 6, 131-135, doi: 10.1088/1742-2132/6/2/004, 2009.

Lawrence, D.M. and Slater, A.G.: A projection of severe near-surface permafrost degradation during the 21st century, Geophy. Res. Lett. , 32, L24401, doi: 10.1029/2005GL025080, 2005.

Lawrence, D.M. and Slater, A.G:. The contribution of snow condition trends to future ground climate, Clim. Dyn., 34, 969-981, doi: 10.1007/s00382-009-0537-4, 2010.

Lebret, P., Dupas, A., Clet, M., Coutard, J., Lautridou, J., Courbouleix, S., Garcin, M., Levy, M., and Van Vliet-Lanoë, B.: Modelling of permafrost thickness during the late glacial stage in France: preliminary results, Can. J. Earth Sci., 31, 959-968, 1994.

Lewkowicz, A.G., Etzelmuller, B., and Smith, S.: Characteristics of discontinuous permafrost based on ground temperature measurements and electrical resistivity tomography, Southern Yukon, Canada, Permafrost Periglac., 22, 320-342, doi: 10.1002/ppp.703, 2011.

Li, X. and Koike, T.: Frozen soil parameterization in SiB2 and its validation with GAME-Tibet observations, Cold Reg. Sci. Technol, 36, 165-182, doi:10.1016/S0165-232X(03)00009-0, 2003.

Ling, F. and Zhang, T.: A numerical model for surface energy balance and thermal regime of the active layer and permafrost containing unfrozen water, Cold Reg. Sci. Technol., 38, 1-15, 2004.Lunardini, V.J. Permafrost formation time, Cold Regions Research and Engineering Laboratory, Hannover, N.H., CRREL Report 95-8, 1995.

Lynch-Stieglitz, M.: The development and validation of a simple snow model for the GISS GCM, J. Climate, 7, 1842–1855, 1994.

McGuffie, K. and Henderson-Sellers, A.: A Climate Modelling Primer, John Wiley & Sons, Ltd., West Sussex, England, 2013.

Nicolsky, N.J., Romanovsky, V.E., and Panteleev, G.G.: Estimation of soil thermal properties using in-situ temperature measurements in the active layer and permafrost, , Cold Reg. Sci. Technol, 55, 120-129, 2009.

Nováková, L., Sosna, K., Brož, M., Najser, J ., and Novák, P.: The matrix porosity and related properties of a leucocratic granite from the Krudum Massif, West Bohemia, Acta Geodyn. Geomater., 9, 521-540, 2012.

Opsteegh, J., Haarsma, R., Selten, F., and Kattenberg, A.: ECBILT: A dynamic alternative to mixed boundary conditions in ocean models, Tellus, 50, 348–367, 1998.

Osterkamp, T.E. and Gosink, J.P.: Variations in permafrost thickness in response to changes in paleoclimate, J. Geophys. Res., 96, 4423-4434, 1991.

Osterkamp, T.E. and Payne, M.W.: Estimates of permafrost thickness from well logs in northern Alaska, Cold Reg. Sci. Technol, 5, 13-27, 1981.

Pitman, A.J., Yang, Z-L., Cogley, J.G., and Henderson-Sellers, A.: Description of bare essentials of surface transfer for the Bureau of Meteorological Research Centre AGCM, BRMC, Australia, BMRC Research Report 32, 117 pp., 1991.

Renssen, H., Goosse, H., Fichefet, T., Brovkin, V., Driesschaert, E., and Wolk, F.: Simulating the Holocene climate evolution at northern high latitudes using a coupled atmosphere-sea ice-ocean-vegetation model, Clim. Dynam., 24, 23–43, doi: 10.1007/s00382-004-0485-y, 2005.

Renssen, H., Seppä, H., Heiri, O., Roche, D. M., Goosse, H., and Fichefet, T.: The spatial and temporal complexity of the Holocene thermal maximum, Nat. Geosci., 2, 411–414, doi: 10.1038/ngeo513, 2009.

Roche, D.M.: $\delta^{18}O$ water isotope in the *i*LOVECLIM model (version 1.0) – Part 1: Implementation and verification, Geosci. Model Dev., 6, 1481-1491, doi:10.5194/gmd-6-1481-2013, 2013.

Roche, D.M., Dokken, T.M., Goosse, H., Renssen, H., and Weber, S.L.: Climate of the last glacial maximum: sensitivity studies and model-data comparison with the LOVECLIM coupled model, Clim. Past, 3, 205-224, 2007.

Roche, D.M., Dumas, C., Bügelmayer, M., Charbit, S., and Ritz, C.: Adding a dynamical cryosphere to *i*LOVECLIM (version 1.0): coupling with the GRISLI ice-sheet model, Geosci. Model Dev., 7, 1377-1394, doi: 10.5194/gmd-7-1377-2014, 2014.

Roche, D.M., Renssen, H., Paillard, D., and Levavasseur, G.: Deciphering the spatio-temporal complexity of climate change of the last deglaciation: a model analysis, Clim. Past, 7, 591-602, doi: 10.5194/cp-3-205-2007, 2011.

Romanovsky, V.E. and Osterkamp, T.E.: Interannual variations of the thermal regime of the active layer and near-surface permafrost in northern Alaska, Permafrost Periglac., 6, 313-335, 1995.

Schaefer, K., Zhang, T., Bruhwiler, L. and Barret, A.P.: Amount and timing of permafrost carbon release in response to climate warming, Tellus Series B Chemical and Physical Meteorology , 63B, 165-180, 2011.

Schild, M., Siegesmund, S., Vollbrecht, A., and Mazurek, M.: Characterization of granite matrix porosity and pore-space geometry by in situ and laboratory methods, Geophys. J. Int., 146, 111-125, 2001.

Shur, Y.L. and Jorgenson, M.T.: Patterns of permafrost formation and degradation in relation to climate and ecosystems, Permafrost Periglac., 18, 7-19, doi: 10.1002/ppp.582, 2007.

Smith, M.W. and Riseborough, D.W.: Climate and the limits of permafrost: A zonal analysis, Permafrost Periglac., 13, 1-15, 2002.

Ter Voorde, M., van Balen, R., Luijendijk, E., and Kooi, H.: Weichselian and Holocene climate history reflected in temperatures in the upper crust of the Netherlands, Neth. J. Geosci., 93, 107-117, doi:10.1017/njg.2014.9, 2014.

Vandenberghe, J., French, H.M., Gorbunov, A., Marchenko, S., Velichko, A.A., Jin, H., Cui, Z., Zhang, T., and Wan, X.: The Last Permafrost Maximum (LPM) map of the Northern Hemisphere: permafrost extent and mean annual temperatures, 25-17 ka BP, Boreas, 43, 652-666, doi: 10.1111/bor.12070, 2014.

Verseghy, D.L.: CLASS-A Canadian land surface scheme for GCMS I. Soil model, Int. J. Climatol., 11, 111-133, 1991.

Wang, G., Mao, T., Chang, J., and Du, J.: Impacts of surface soil organic content on the soil thermal dynamics of alpine meadows in permafrost regions: data from field observations, Geoderma, 232-234, 414-425, doi: 10.1016/j.geoderma.2014.05.016, 2014.

Weber, S.L.: The utility of Earth system Models of Intermediate Complexity (EMICs), WIREs Climate Change, 1, 243-252, doi: 10.1002/wcc.24, 2010.

Williams, D.J. and Burn, C.R.: Surficial characteristics associated with the occurrence of permafrost near Mayo, Central Yukon Terrritory, Canada, Permafrost Periglac., 7, 193-206, 1996.

Williams, P.J. and Smith, M.W.: The Frozen Earth: Fundamentals of Geocryology, Cambridge University Press, Cambridge, England, 2007.

Woo, M.K. and Xia, Z.: Effects of hydrology on the thermal conditions of the active layer, Nordic Hydrology, 27, 129–142, 1996.

Zemtsov, A.A. and Shamakhov. A.F.: Characteristics of relict permafrost on the west Siberian plain, Polar Geography and Geology, 17, 245-250, 1993.

Zhang, T.: Influence of the seasonal snow cover on the ground thermal regime: an overview, Rev. Geophys., 43, RG4002, doi:10.1029/2004RG000157, 2005.

Zhang, Y., Carey, S.K., and Quinton, W.L.: Evaluation of the algorithms and parameterizations for ground thawing and freezing simulation in permafrost regions. J. Geophys. Res., 113, D17116, DOI: 10.1029/2007JD009343, 2008.

Zhang, Y., Chen, W., and Riseborough, D.: Temporal and spatial changes of permafrost in Canada since the end of the Little Ice Age. J. Geophys. Res., 111, doi:10.1029/2006JD007284, 2006.

Table 1. Variable values applied in the Stefan equation.

Variables		
thermal conductivity (k_{mw})	1.7	W m^{-1} K^{-1}
dry density of soil (ρ_m)	1600	kg m^{-3}
latent heat of fusion (L)	334	kJ kg^{-1}
total moisture content (W)	0.3	-
unfrozen water conent (W_u)	0	-

Table 2. Calculated maximum annual active layer thickness using both the Stefan Equation and the VAMPER model under different forcing scenarios.

Model Run	Average Annual Ground Surface Temperature	Annual Amplitude	Stefan Equation Active Layer	Vamper Model Active Layer
	(°C)	**(°C)**	**(m)**	**(m)**
1	-6	10	0.7	0.7
2	-4	10	1.0	1.0
3	-2	10	1.2	1.3
5	-6	20	1.6	1.7
6	-4	20	1.7	1.9
7	-2	20	1.9	1.9

Table 3. The original lithological classification from Hartmann and Moosdorf (2012) and the reclassification scheme used for the ECBilt grid.

	Original Litho Class	VAMPER Class
1	Unconsolidated Sediments (SU)	Sed
2	Basic Volcanic Rocks (VB)	Bed
3	Siliciclastic Sedimentary Rocks (SS)	Sed
4	Basic Plutonic Rocks (PB)	Bed
5	Mixed Sedimentary Rocks (SM)	Sed
6	Carbonate Sedimentary Rocks (SC)	Sed
7	Acid Volcanic Rocks (VA)	Bed
8	Metamorphic Rocks (MT)	Bed
9	Acid Plutonic Rocks (PA)	Bed
10	Intermediate Volcanic Rocks (VI)	Bed
11	Water Bodies (WB)	N/A
13	Pyroclastics (PY)	Bed
12	Intermediate Plutonic Rocks (PI)	Bed
15	Evaporites (EV)	Sed
14	No Data (ND)	N/A
16	Ice and Glaciers (IG)	N/A

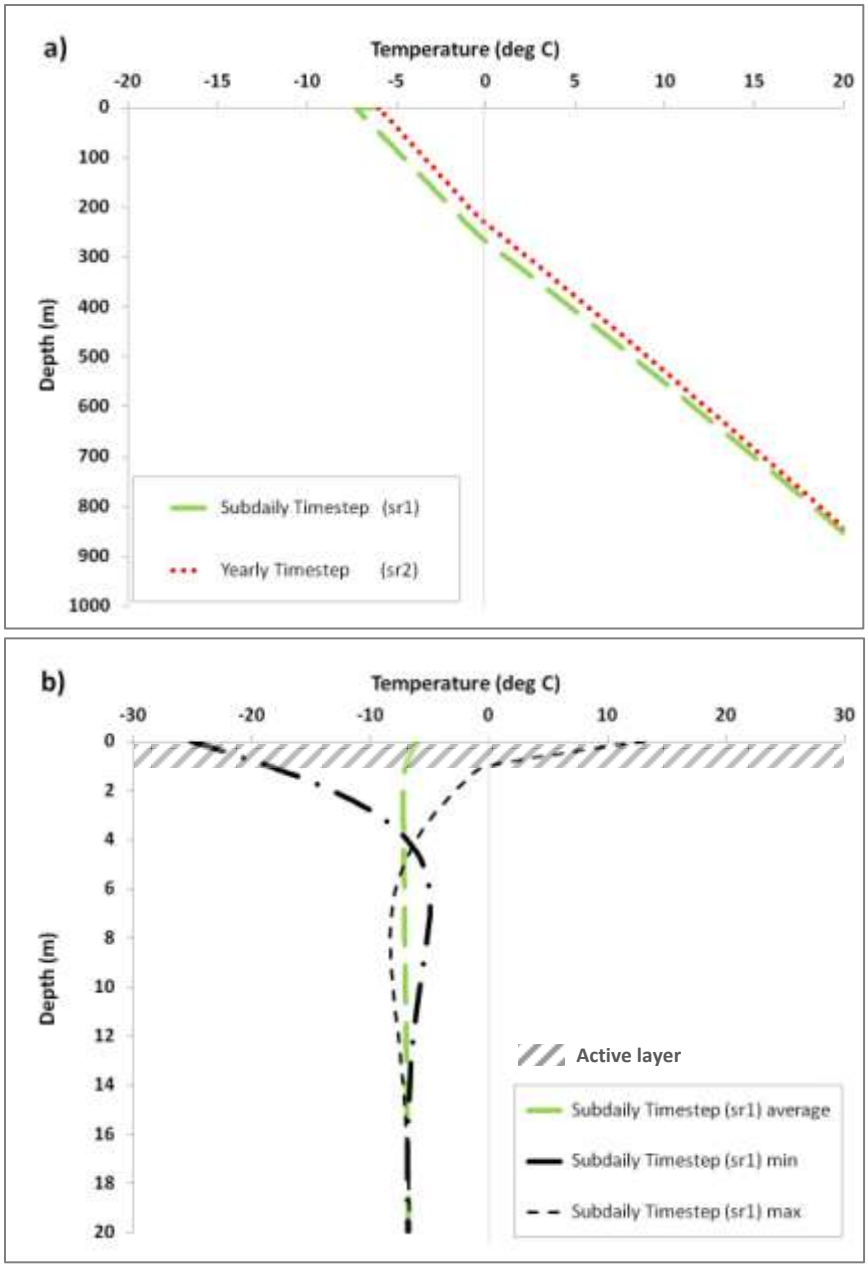

Figure 1. a) Plot comparing VAMPER model results using different timesteps (annual vs. subdaily) but the same annual average temperature forcing of -6 °C. b) Plot showing the sr1 average, min, and max temperature-depth profiles. Also shown in b) is the ~ 1 m active layer, marked as diagonal lines.

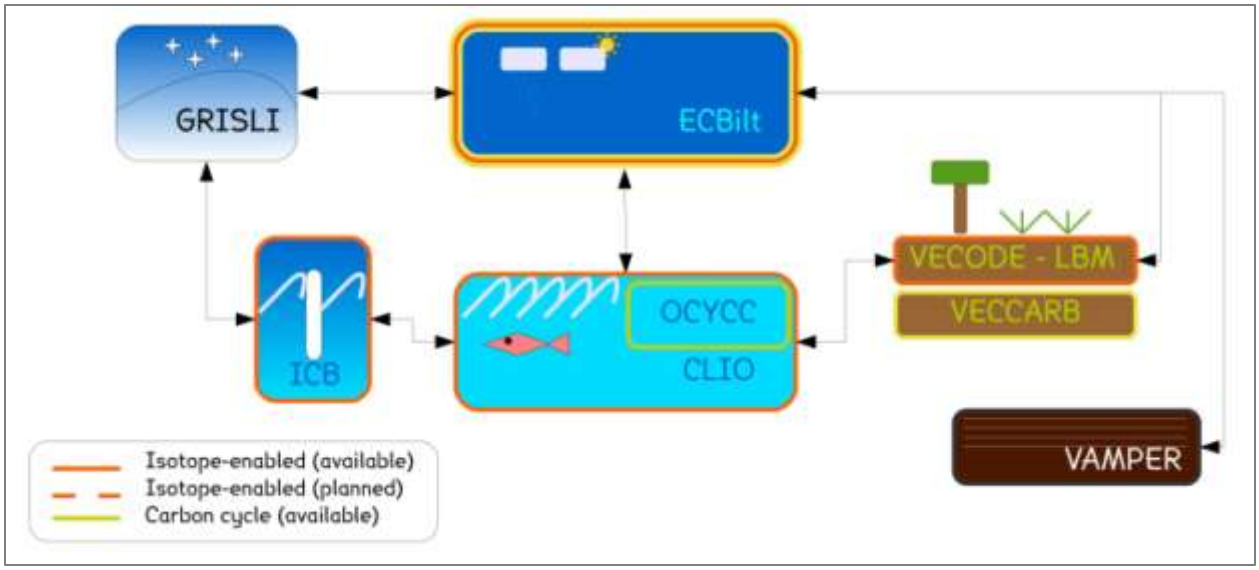

Figure 2. *i*LOVECLIM model component setup.

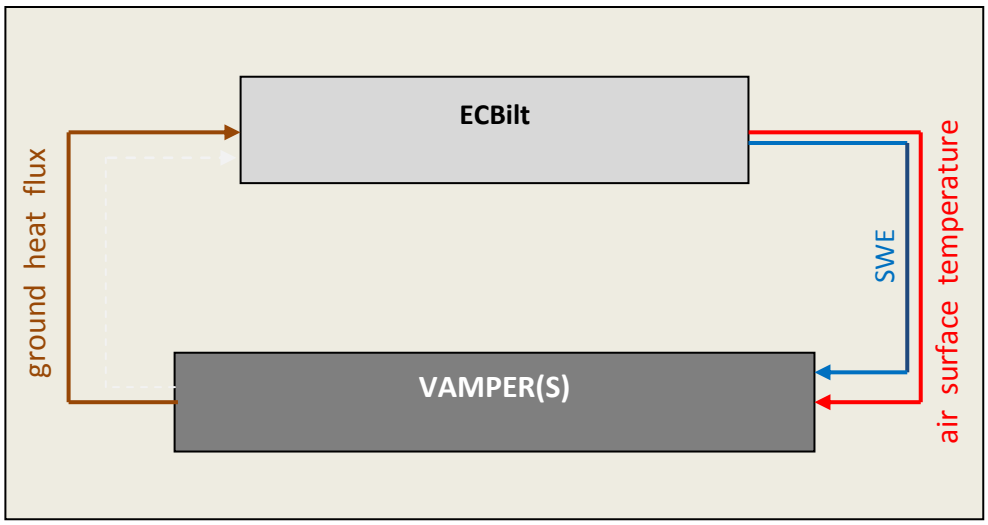

Figure 3. Coupling scheme between ECBilt and the VAMPER(S) model showing the variables (air surface temperature, swe, and ground heat flux) passed between the components at each timestep.

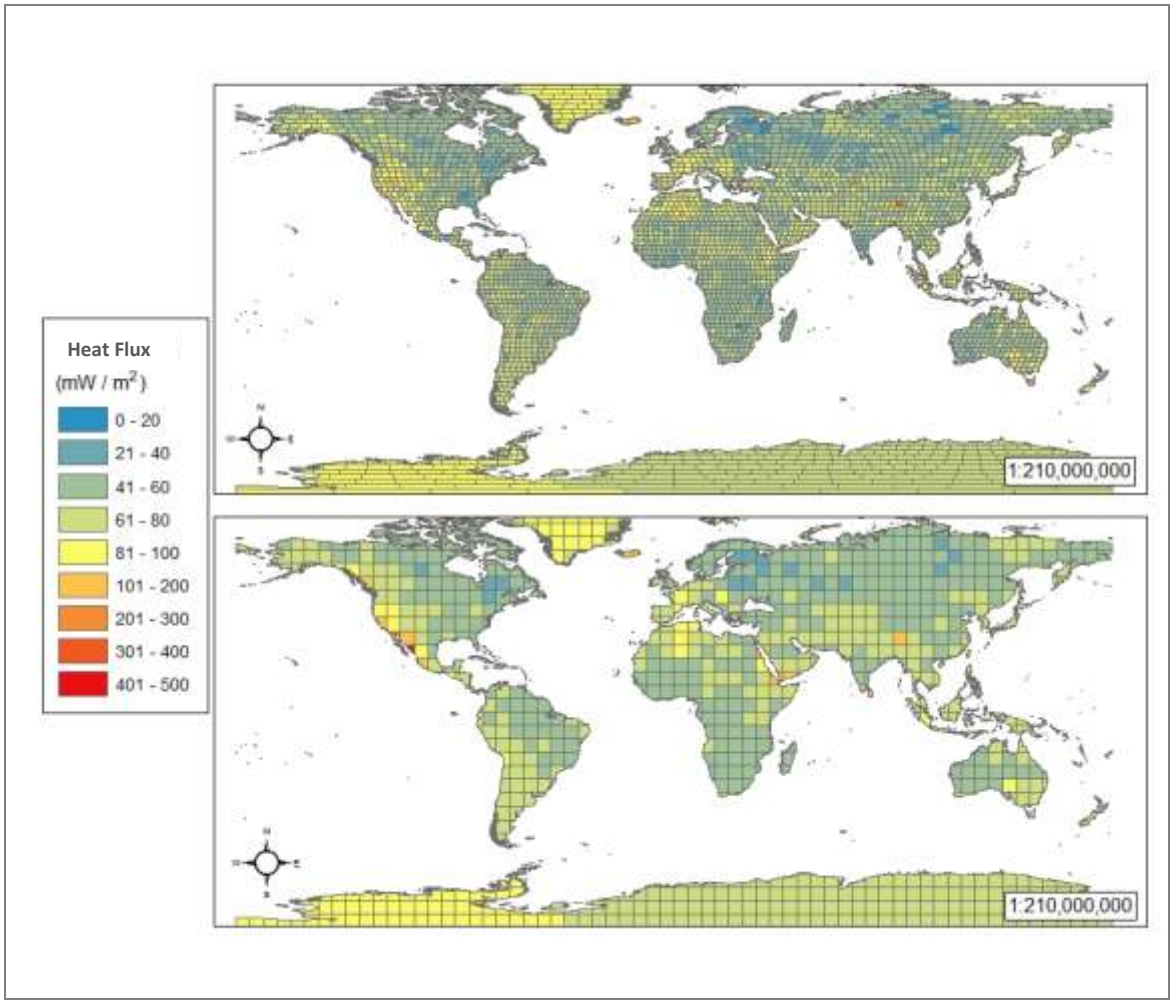

Figure 4. The original geothermal heat flux map (top) from Davies (2013) and the weighted average version (top) for use as the lower boundary value in the *i*LOVECLIM experiments (bottom).

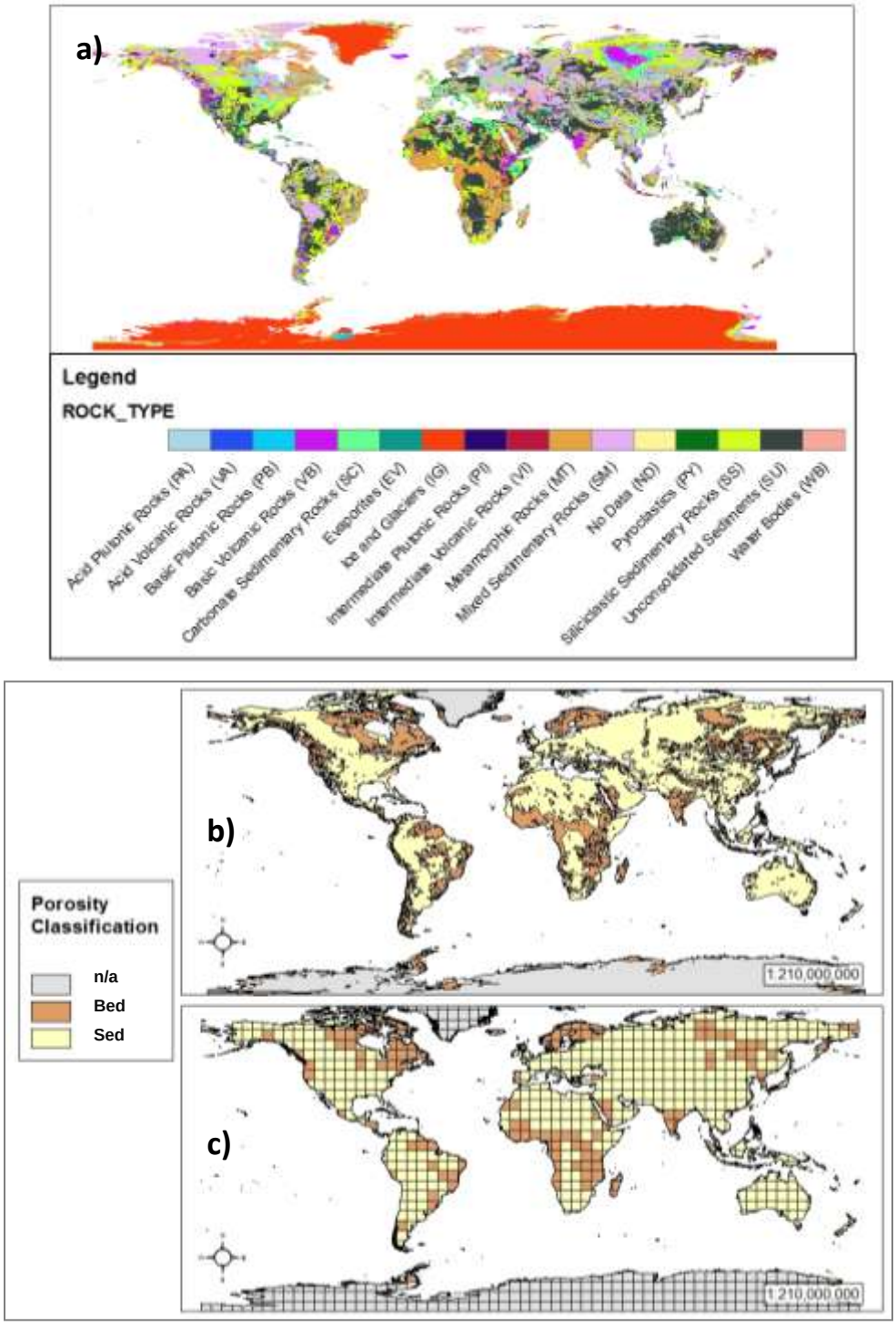

Figure 5. World maps showing a) original map from Hartmann and Moosdorf (2012) b) map of reclassified lithology using Table 2 and c) the version geo-processed to match the ECBilt grid resolution.

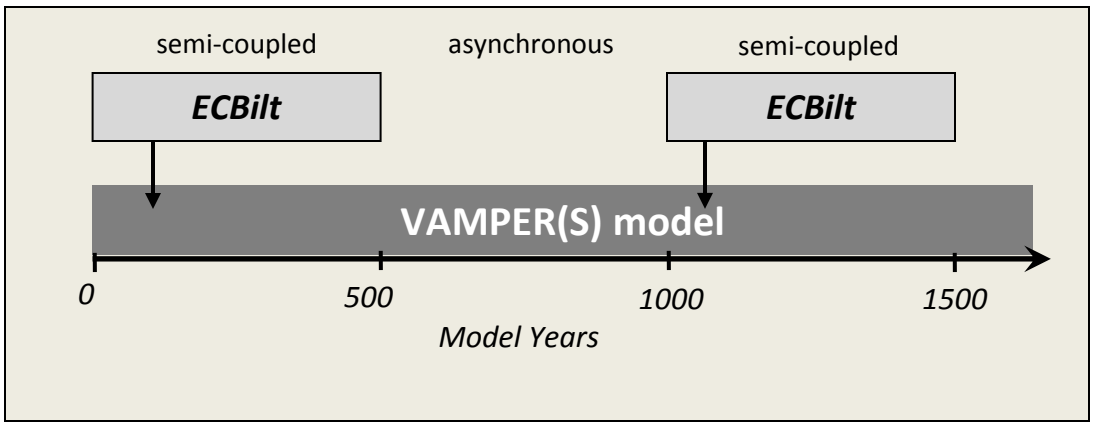

Figure 6. An illustration of asynchronous coupling between VAMPER(S) and ECBilt. The components are run semi-coupled for 100 years while VAMPER(S) is run the entire time. This allows VAMPER(S) to equilibrate with the climate state of *i*LOVECLIM using less computer resources time than a synchronous version.

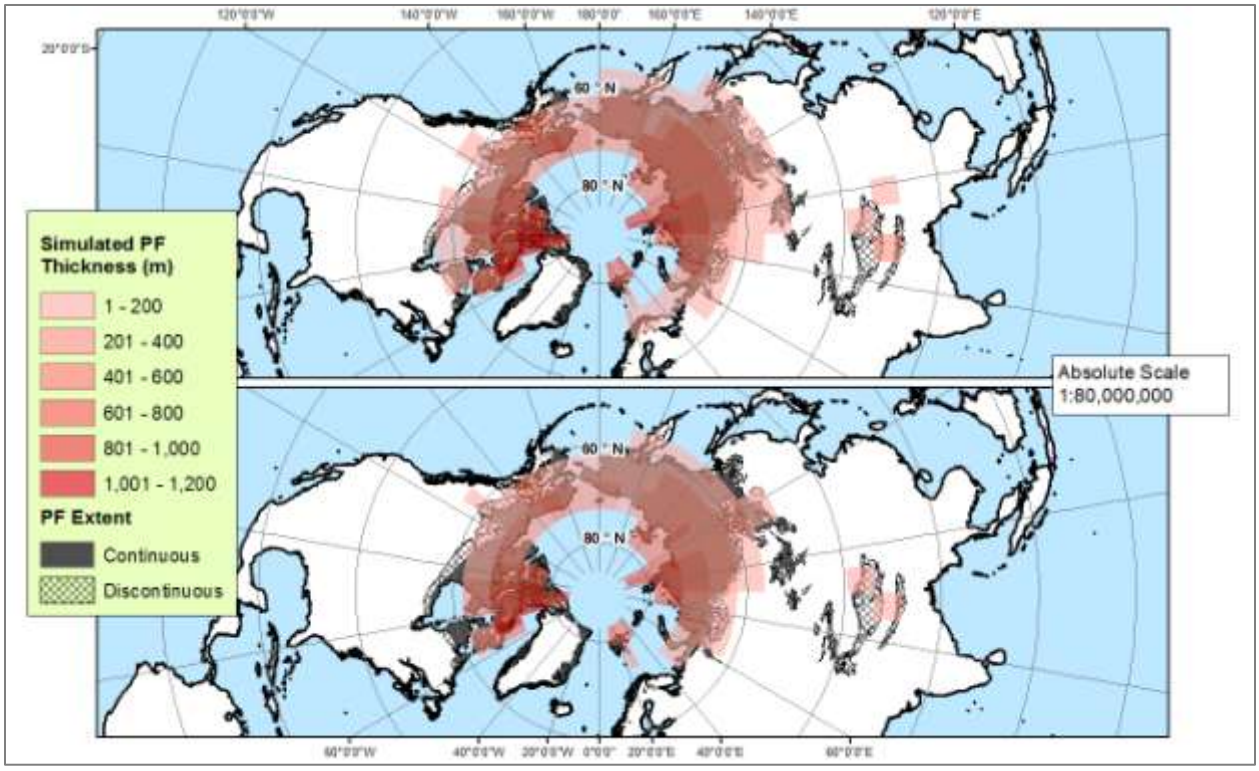

Figure 7. Preindustrial simulation results for permafrost thickness distribution using ECBILT-VAMPER semi-coupling (top) and ECBILT-VAMPERS semi-coupling (bottom).

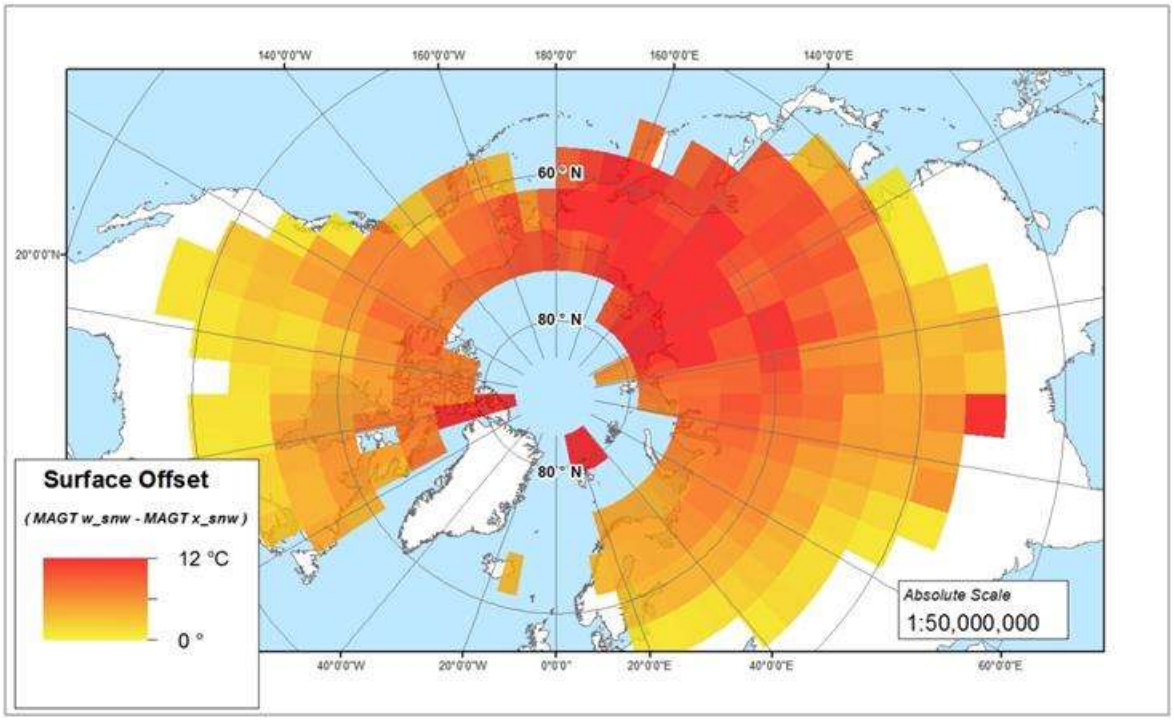

Figure 8. Mean annual surface offset as a result of including the snow option in the ECBilt-VAMPERS coupling.

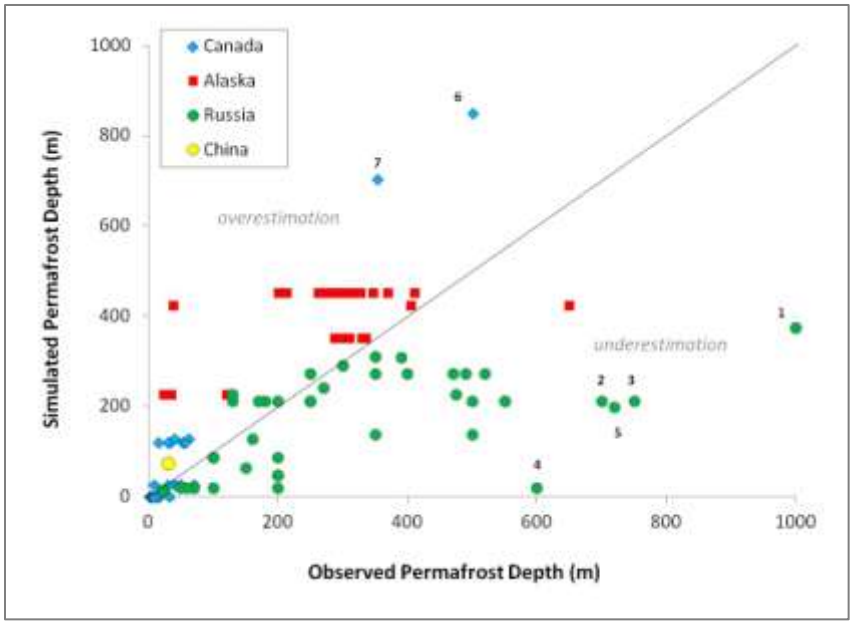

Figure 9. A 1:1 scatterplot comparing simulated thickness results with corresponding permafrost thickness estimates from borehole data. Points 1-7 are outliers mentioned specifically above.

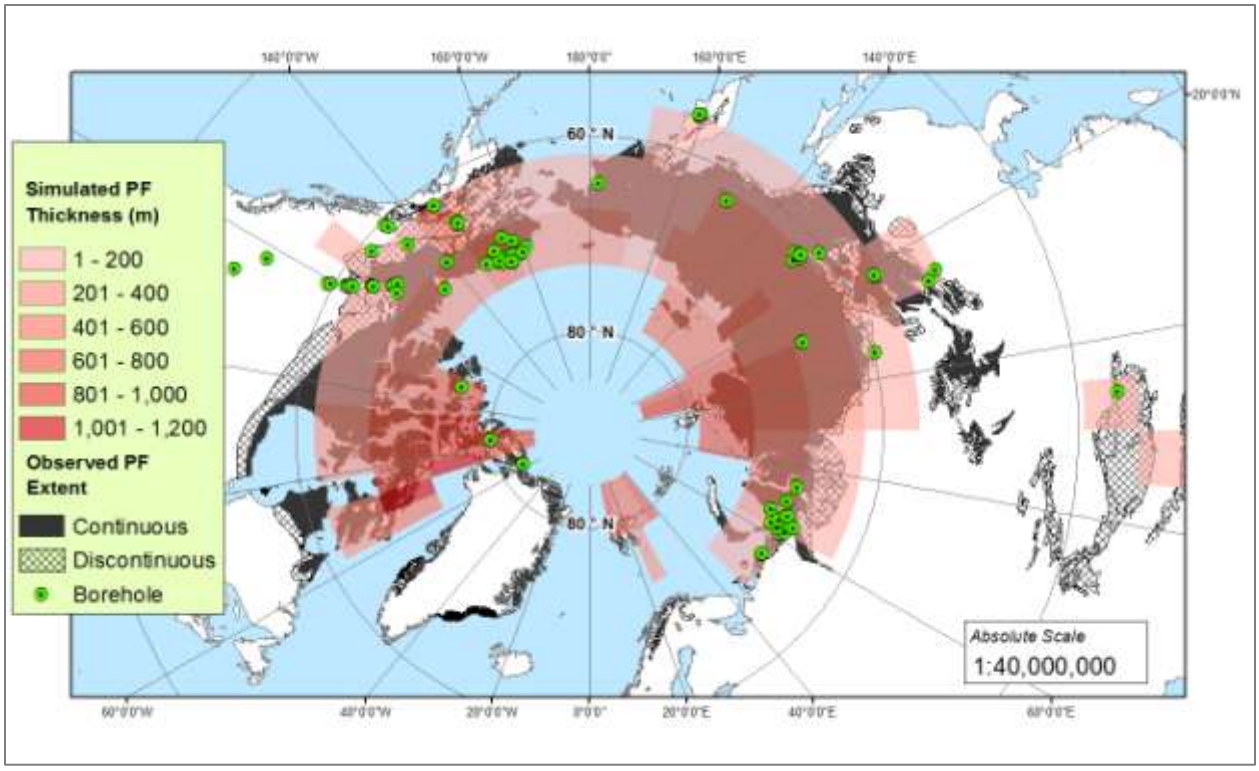

Figure 10. Map of deep GTN-P borehole locations with the simulated permafrost thickness (with snow enhancement) and observed PF extent (Brown et al., 2014).

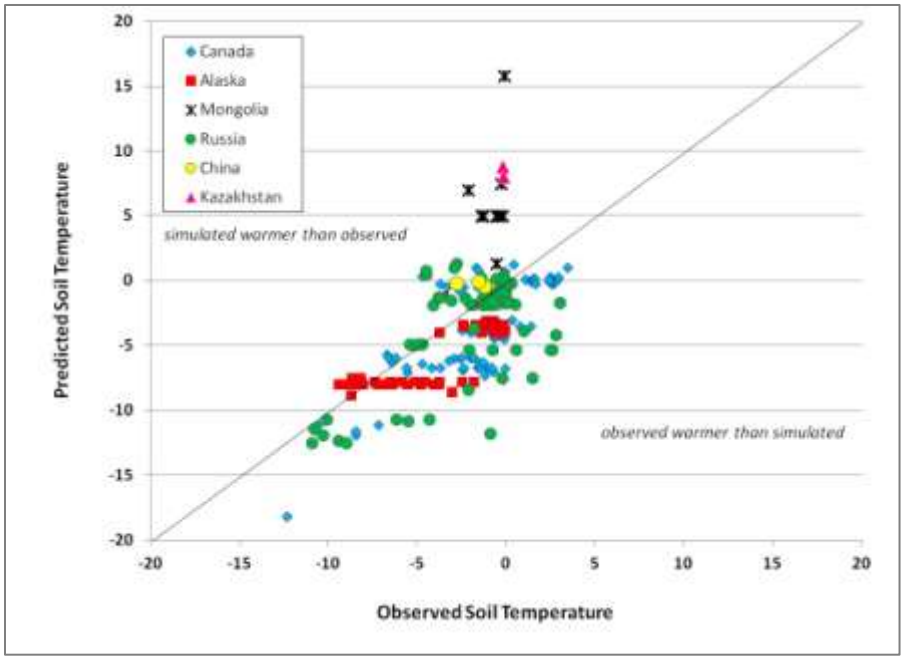

Figure 11. A 1:1 scatterplot comparing simulated mean annual temperatures with corresponding MAGT measurements.

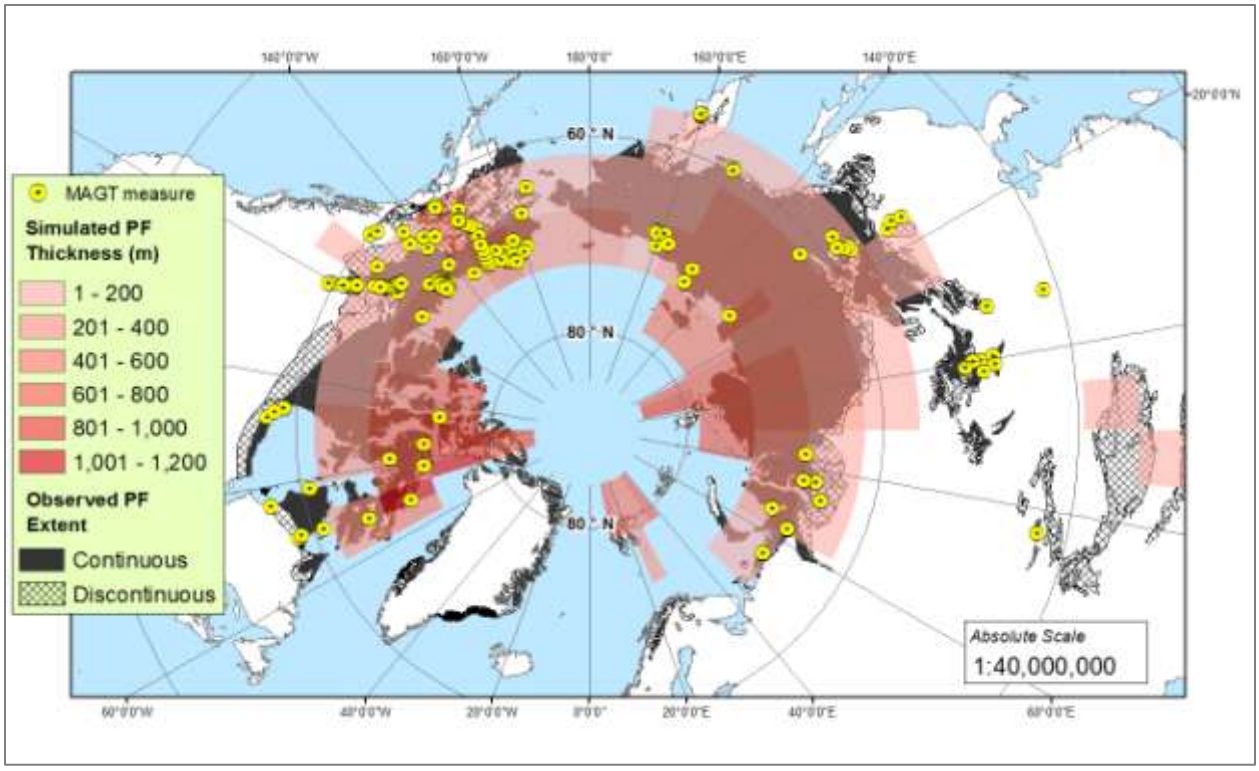

Figure 12. Map showing locations of the MAGT measurements, collected for the IPY 2010 (GTN-P), used in the comparison to corresponding *i*LOVECLIM simulated subsurface temperatures.